Part 3

Optical Properties of Particles

Chapter 11
Extinction

Extinction is the attenuation of an electromagnetic wave by scattering and absorption as it traverses a particulate medium. In homogeneous media the dominant attenuation mechanism is usually absorption. Comparison of extinction spectra for small particles of various sizes with absorption spectra for the bulk parent material reveals both similarities and differences; we shall make such comparisons in the early part of this chapter. After reviewing the meaning of extinction and the various ways it is commonly presented (Section 11.1), we survey extinction effects in particles of the three illustrative materials of Chapter 10 (Section 11.2). Following this survey, the major features of spectral extinction (except those reserved for Chapter 12) are discussed in more detail: extinction dominated by scattering, including size and size distribution effects (Section 11.3); ripple structure (Section 11.4); and the effects of absorption (Section 11.5). Calculations of extinction by spheroids and infinite cylinders in Section 11.6 are followed in Section 11.7 by measurement techniques and experimental results for both spherical and nonspherical particles. We conclude with a brief summary in Section 11.8.

11.1 EXTINCTION = ABSORPTION + SCATTERING

If multiple scattering is negligible the irradiance of a beam of light is exponentially attenuated from I_i to I_t in traversing a distance h through a particulate medium (see Section 3.4):

$$\frac{I_t}{I_i} = \exp(-\alpha_{\text{ext}} h). \tag{11.1}$$

Extinction is the result of both absorption and scattering:

$$\alpha_{\text{ext}} = \mathcal{N}(C_{\text{abs}} + C_{\text{sca}}); \tag{11.2}$$

$\mathcal{N}$ is the number of particles per unit volume; C_{abs} and C_{sca} are the absorption and scattering cross sections. Although both processes occur simultaneously, there are instances where one or the other dominates. For example, visible light passing through a fog is attenuated almost entirely by scattering, whereas light passing along the shaft of a coal mine might be attenuated primarily by absorption. A simple but effective demonstration of these two extremes,

particularly well suited to large audiences, is shown schematically in Fig. 11.1. Two transparent containers (Petri dishes serve quite well) are filled with water, placed on an overhead projector, and their images focused on a screen. To one container, a few drops of milk are added; to the other, a few drops of India ink. The images can be changed from clear to a reddish hue to black by increasing the amount of milk or ink. Indeed, both images can be adjusted so that they appear equally dark; in this instance it is not possible, judging solely by the light transmitted to the screen, to distinguish one from the other: the amount of extinction is about the same. But the difference between the two suspensions immediately becomes obvious if one looks directly at the containers: the milk is white whereas the ink is black. Milk is a suspension of very weakly absorbing particles which therefore attenuate light primarily by scattering; India ink is a suspension of very small carbon particles which attenuate light primarily by absorption. Although this demonstration is not meant to be quantitative, and its complete interpretation is complicated somewhat by multiple scattering, it clearly shows the difference between extinction by scattering and extinction by absorption. Moreover, it shows that merely by observing transmitted light it is not possible to determine the relative contributions of absorption and scattering to extinction; to do so requires an additional independent observation.

Extinction of light by particles is a fairly commonly observed phenomenon: sunlight through a dust storm or a polluted layer of air; automobile headlights in fog; a skin diver's light in murky water. All these examples of extinction, however, are not necessarily described by the theoretical expressions (11.1) and (11.2). Multiple scattering aside, underlying (11.2) is the assumption that *all* light scattered by the particles, however small the scattering angle, is excluded from the detector. But the eye, or any other detector, collects light scattered in

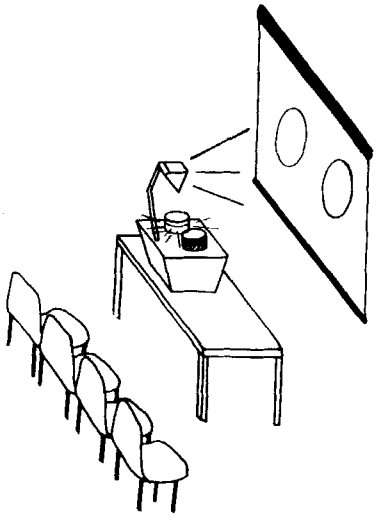

Figure 11.1 A demonstration of how extinction may be dominated either by scattering or by absorption: one Petri dish contains a milk suspension; the other contains an India ink suspension.

some possibly small but finite set of angles around the forward direction; the larger the particles the more the scattering diagram is peaked in the forward direction and the greater the possible discrepancy between measured and calculated extinction. Thus, a detection system may have to be carefully designed to measure extinction that can be legitimately compared with theoretical extinction, particularly by large particles. Extinction by interstellar dust is an example where the requirements of theory are most likely to be strictly satisfied: distances to particles are thousands of light years and a detector coupled to a telescope receives almost entirely light that has not been scattered.

There is not a unique way of representing extinction. Physicists, because they are accustomed to cross sections for various atomic and nuclear processes, are probably most comfortable with the extinction cross section $C_{ext} = C_{abs} + C_{sca}$. On the other hand, the extinction efficiency $Q_{ext} = C_{ext}/(\text{cross-sectional area})$ is more likely to bring a smile to the face of an astronomer or an atmospheric scientist. In the books by van de Hulst (1957) and Kerker (1969), extinction efficiencies are presented almost exclusively; consequently, this has become widespread. But we argued in Section 3.4 that the extinction cross section per unit particle volume (or mass) may be a more appropriate measure of how efficiently a particle attenuates light. These three ways of representing extinction, which are listed below, may be looked upon as merely different ways of normalizing the extinction cross section.

Cross section	C_{ext}	$Q_{ext}\pi a^2$ (sphere)
Cross section per unit area	C_{ext}/A	Q_{ext}
Cross section per unit volume	C_{ext}/V	$3Q_{ext}/4a$ (sphere)

Plots of each of these quantities as a function of particle size would look quite different and, therefore, would tell different stories. Except for a scale factor, each of them plotted as a function of wavelength for the same particle size would be identical. In our first example of extinction (Fig. 4.6) we displayed the efficiency Q_{ext}, as we shall often do in this chapter. In Chapter 12, however, our preference switches to the extinction cross section per unit particle volume. Unnormalized extinction cross sections (strictly speaking, the differential scattering cross section integrated over the acceptance angle of the detector) are more appropriate in Section 13.5 on particle sizing.

11.2 EXTINCTION SURVEY

Curves of extinction as a function of size parameter show a wealth of features, even when calculated with uninteresting constant optical constants, as has often been done. When realistic optical constants are used in calculations the different types of extinction effects become even more numerous. In this section we incorporate optical constants of the three illustrative materials of

Chapter 10 with Mie theory in a survey of extinction effects which we shall discuss in more detail in subsequent sections.

11.2.1 Magnesium Oxide

Volume-normalized extinction is plotted in Fig. 11.2 as a function of photon energy for several polydispersions of MgO spheres; both scales are logarithmic. For comparison of bulk and small-particle properties the bulk absorption coefficient $\alpha = 4\pi k/\lambda$ is included. Some single-particle features, such as ripple structure, are effaced by the distribution of radii. The information contained in these curves is not assimilated at a glance: they require careful study.

At and near visible wavelengths, where bulk MgO is highly transparent, extinction is dominated by scattering. As a consequence, attenuation by MgO particles is quite different from that by the bulk solid. If the particles are much smaller than the wavelength, scattering varies as the fourth power of the photon energy ($1/\lambda^4$); at such wavelengths extinction is a linear function of photon energy on a logarithmic plot. Greater extinction of higher than lower energy light gives rise to reddening, which may be observed in light transmitted through an MgO-smoked microscope slide. If the particles are large compared with the wavelength, extinction dominated by scattering is nearly independent of photon energy. Note in particular the broad range of neutral extinction for the particles with mean radius 1.0 μm. White light would undergo little discernible change in color upon transmission by such particles.

At energies where MgO electronic absorption sets in, structure in the bulk optical constants appears in extinction (both scattering and absorption), but only for the smallest particles (0.01 μm). No structure is apparent in the extinction spectrum of particles with mean radius 0.05 μm at energies greater than about 7.6 eV. At these energies the particles are "black": no appreciable light that penetrates the particles reemerges carrying the spectral information. This effect could be called "saturation", although this term is used in many different ways.

Because the particles must be very small, not more than a few hundred angstroms for most substances, there have been few laboratory observations of structure in ultraviolet extinction spectra of small, nonmetallic particles. Particles of the required size are difficult to make. Grinding them from the bulk, with the attendant problem of separation, is almost hopeless. Various smokes can be made, MgO particularly easily, but not of all substances that might be of interest.

Extinction and absorption spectra for 0.01 μm particles with optical constants appropriate to radiation-damaged MgO (see Fig. 10.1) are also shown in Fig. 11.2. The lowest-energy absorption band among the three broad bands shows clearly in extinction but not the highest-energy band. In this instance obscuration of structure is caused by the dominance of scattering over absorption, not "saturation" of absorption. This is obvious from the absorption spectrum, in which all three bands are evident. To observe the band at 3.5 eV

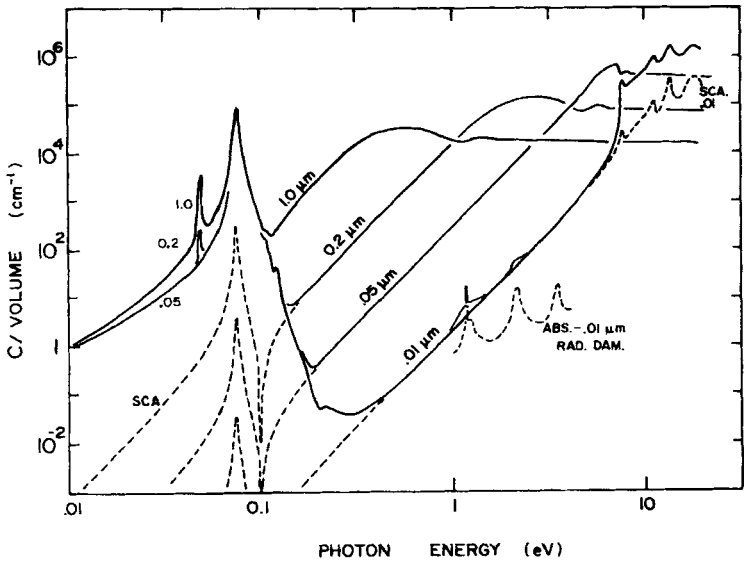

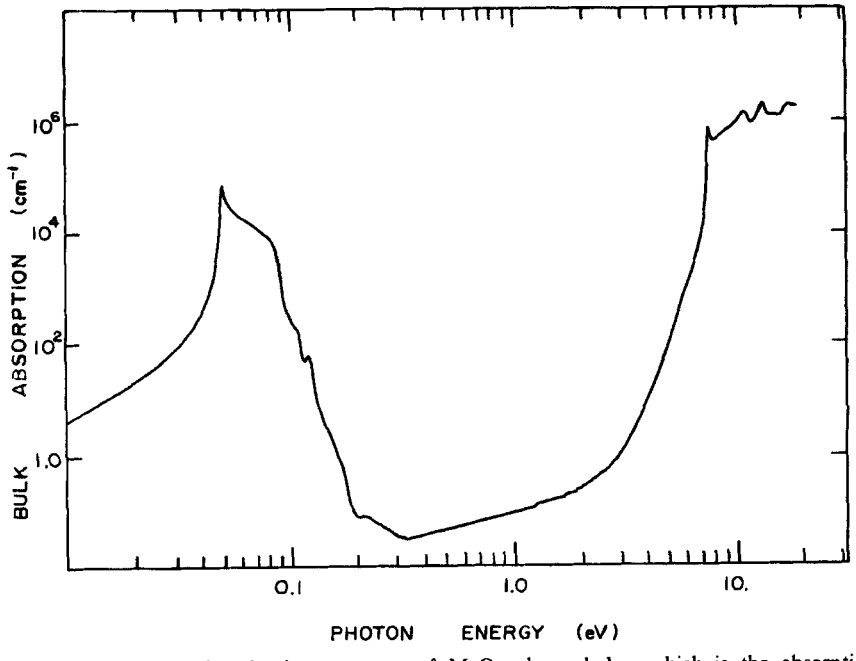

Figure 11.2 Calculated extinction spectrum of MgO spheres below which is the absorption spectrum of bulk MgO.

would require measuring absorption in the presence of a large amount of scattering. Diffuse reflectance techniques (Kortüm, 1969) or the increasingly popular photoacoustic spectroscopy (Rosencwaig, 1980) could be used. These techniques, however, would be applied less successfully to absorption bands between 7 and 20 eV for 0.05-μm particles or larger.

At infrared wavelengths extinction by the MgO particles of Fig. 11.2, including those with radius 1 μm, which *can* be made by grinding, is dominated by absorption. This is why the KBr pellet technique is commonly used for infrared absorption spectroscopy of powders. A small amount of the sample dispersed in KBr powder is pressed into a pellet, the transmission spectrum of which is readily obtained. Because extinction is dominated by absorption, this transmission spectrum should follow the undulations of the intrinsic absorption spectrum—but not always. Comparison of Figs. 10.1 and 11.2 reveals an interesting discrepancy: calculated peak extinction occurs at 0.075 eV, whereas absorption in bulk MgO peaks at the transverse optic mode frequency, which is about 0.05 eV. This is a large discrepancy in light of the precision of modern infrared spectroscopy and could cause serious error if the extinction peak were assumed to lie at the position of a bulk absorption band. This is the first instance we have encountered where the properties of small particles deviate appreciably from those of the bulk solid. It is the result of surface mode excitation, which is such a dominant effect in small particles of some solids that we have devoted Chapter 12 to its fuller discussion.

The scattering cross section in Fig. 11.2 also peaks at about 0.075 eV, although it is much less than the corresponding absorption cross section. Note that the scattering cross section drops sharply near 0.1 eV, where the real part of the refractive index is about 1 and the imaginary part is low: the particles are almost optically identical with free space. This is the *Christiansen effect*, which can be exploited to make a band-pass filter (see, e.g., Smith et al., 1968, pp. 395–399). Transmission through a collection of particles is greatest near the Christiansen frequency (where $n = 1$ and $k \simeq 0$) because scattering nearly vanishes; at neighboring frequencies scattering greatly diminishes the transmitted light. Larger particles than we have discussed in connection with Fig. 11.2 are required, however, so that absorption does not dominate over scattering.

11.2.2 Water

Mie calculations with the optical constants of water given in Fig. 10.3 are shown in Fig. 11.3; extinction and absorption are plotted logarithmically, photon energy linearly. The bulk absorption coefficient of water is shown in Fig. 11.3*c*. Because many of the extinction features of water and MgO, both of which are insulators, are similar, we present calculations for a single water droplet (in air) with radius 1.0 μm. Size-dependent spectral features are therefore not obscured as they are for a distribution of radii.

Perhaps the most conspicuous features in extinction appear where water is transparent, between about 0.5 and 7 eV. Interference of incident and

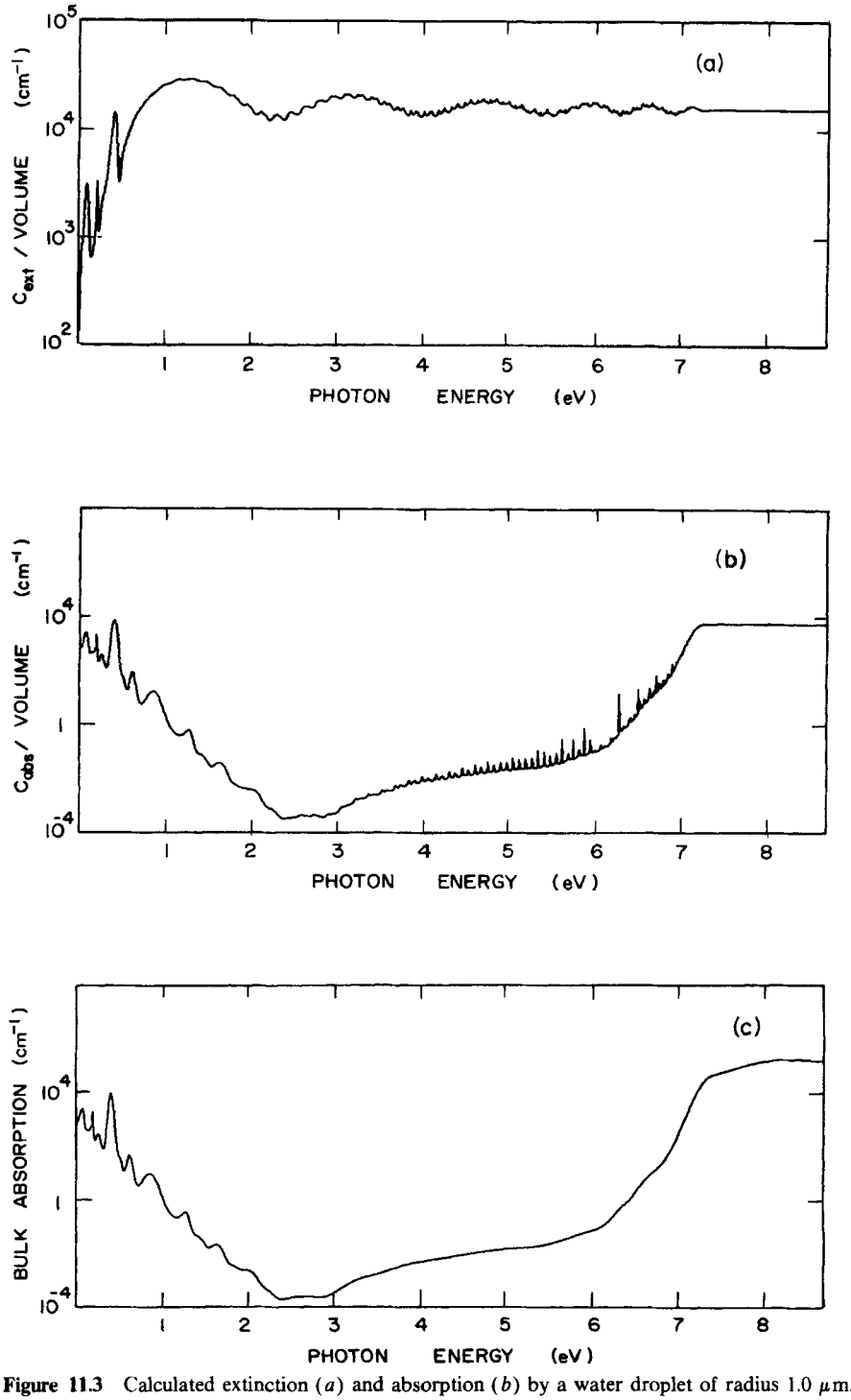

Figure 11.3 Calculated extinction (*a*) and absorption (*b*) by a water droplet of radius 1.0 μm. The absorption spectrum of water is shown in (*c*).

forward-scattered light (see Section 4.4) gives rise to *interference structure*: a series of broad, regularly spaced extinction maxima and minima. Superimposed on this is sharp and highly irregular *ripple structure*, which originates in resonant electromagnetic modes of a sphere. We shall discuss interference and ripple structure in more detail in Sections 11.3 and 11.4. Since the positions of these features are size dependent (especially ripple structure) they tend not to appear in calculations for polydispersions. This is why the extinction curves for MgO (Fig. 11.2) are so different from the extinction curve in Fig. 11.3. Also included in this figure is the absorption cross section per unit particle volume. Interference structure does not appear in absorption but ripple structure does, although at energies where absorption is very small. Comparison of the curves for a water droplet (*a* and *b*) with that for water (*c*) shows that interference and ripple structure give to a droplet spectral features which contrast markedly with those of its parent material.

The extinction features at energies where water is transparent are rapidly squelched in the ultraviolet as the onset of electronic transitions greatly increases bulk absorption. In the infrared, however, vibrational absorption bands in water are carried over into similar bands in extinction (dominated by absorption if $a \ll \lambda$) by a water droplet. Unlike MgO there are no appreciable spectral shifts in going from the bulk to particulate states. The reason for this lies in the strength of bulk absorption and will be discussed more thoroughly in Chapter 12.

11.2.3 Aluminum

The calculated extinction spectrum of a polydispersion of small aluminum spheres (mean radius 0.01 μm, fractional standard deviation 0.15) is shown in Fig. 11.4; both scales are logarithmic. In some ways spectral extinction by metallic particles is less interesting than that by insulating particles, such as those discussed in the preceding two sections. The free-electron contribution to absorption in metals, which dominates other absorption bands, extends from radio to far-ultraviolet frequencies. Hence, extinction features in the transparent region of insulating particles, such as ripple and interference structure, are suppressed in metallic particles because of their inherent opacity. But extinction by metallic particles is not without its interesting aspects.

Note that there is *no bulk absorption band* in aluminum corresponding to the prominent extinction feature at about 8 eV. Indeed, the extinction maximum occurs where bulk absorption is monotonically decreasing. This feature arises from a resonance in the collective motion of free electrons constrained to oscillate within a small sphere. It is similar to the dominant infrared extinction feature in small MgO spheres (Fig. 11.2), which arises from a collective oscillation of the lattice ions. As will be shown in Chapter 12, these resonances can be quite strongly dependent on particle shape and are excited at energies where the real part of the dielectric function is negative. For a metal such as aluminum, this region extends from radio to far-ultraviolet frequencies. So the

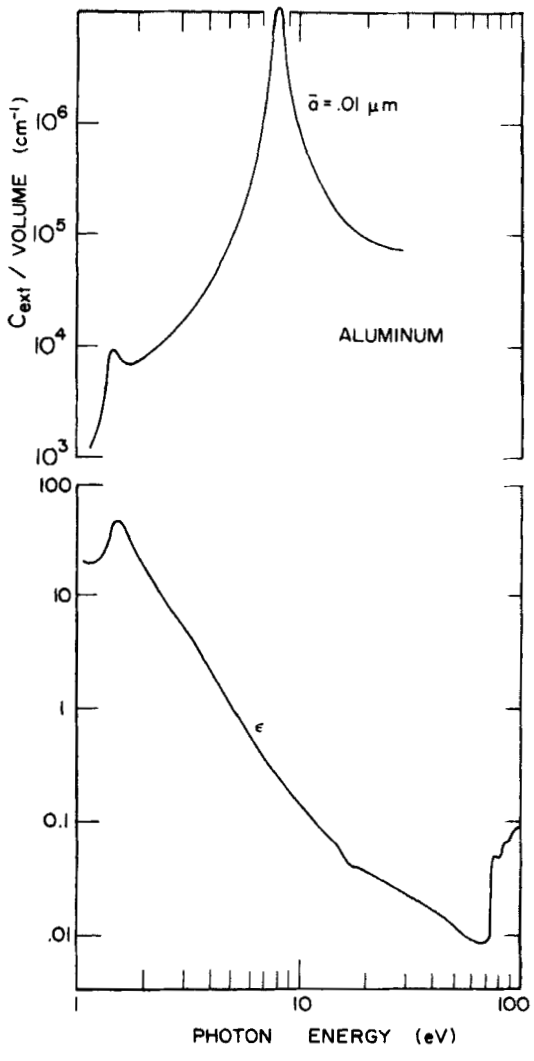

Figure 11.4 Calculated extinction by a polydispersion of aluminum spheres (top) compared with the bulk absorption spectrum of aluminum (bottom).

possible range of shape-dependent features in extinction spectra of small metallic particles is correspondingly broad.

11.3 SOME EXTINCTION EFFECTS IN INSULATING SPHERES

In the preceding section and elsewhere we have touched on a few points that deserve further elaboration. For example, we have emphasized that extinction calculations should, in general, be done with wavelength-dependent optical

constants; in this section we examine the consequences of not doing so. Then we go on to consider the progressive obliteration of features in extinction by a polydispersion of spheres as the spread of their radii is increased.

11.3.1 Two Views of Extinction

Two curves showing extinction by a sphere are given in Fig. 11.5. The refractive index for the top curve is $1.33 + i10^{-8}$, which corresponds to water at about 5600 Å. This is the type of extinction curve most commonly encountered, although it is easy to misinterpret. It strictly represents the dependence of extinction on radius at a *fixed* wavelength, not its dependence on wavelength, despite the fact that the abscissa is proportional to $1/\lambda$. The reason for this is that the optical constants of water—indeed, any substance—depend on wavelength. Only if a suitable refractive index $m(\lambda)$ is incorporated with Mie theory can a calculated curve faithfully show how extinction varies with wavelength, and then only for a single size. This type of curve, for a particle of radius 1.0 μm, is shown in Fig. 11.5*b*.

Comparison of the two curves in Fig. 11.5 reveals both similarities and differences. In the transparent region, between about $x = 3$ and $x = 37$, the extinction features are qualitatively similar but the positions of the major (interference) peaks may be appreciably displaced. The positions of the first peaks (near $x = 7$) are almost identical. But the second peaks are slightly shifted and the third- and higher-order peaks are considerably shifted. This progressively increasing displacement of peak positions is a result of the increase of the real part of the refractive index of water toward the ultraviolet. In the regions where water is absorbing—infrared and ultraviolet—the two curves show little similarity. At $x = 37$ ripple structure abruptly vanishes from the extinction curve of Fig. 11.5*b*; this results from the strong electronic absorption that sets in shortward of about 0.2 μm, the absorption edge. A similar effect occurs for all nonmetallic solids and liquids, although the position of the absorption edge—in or near the ultraviolet—is different for each substance. At values of x less than about two extinction features in Fig. 11.5*b* do not have counterparts in Fig. 11.5*a*; these features arise from the infrared absorption bands of water.

11.3.2 Size Distribution Effects

Extinction features that strongly depend on particle size will be obscured, if not totally obliterated, in a polydispersion. Many analytical expressions for the radius probability distribution have been used in Mie calculations. For purposes of illustration we have chosen the Gaussian distribution, according to which the probability that a sphere has radius between a and $a + da$ is

$$\frac{1}{\sigma\sqrt{2\pi}} \exp\left[-\frac{1}{2}\left(\frac{a-\bar{a}}{\sigma}\right)^2\right] da,$$

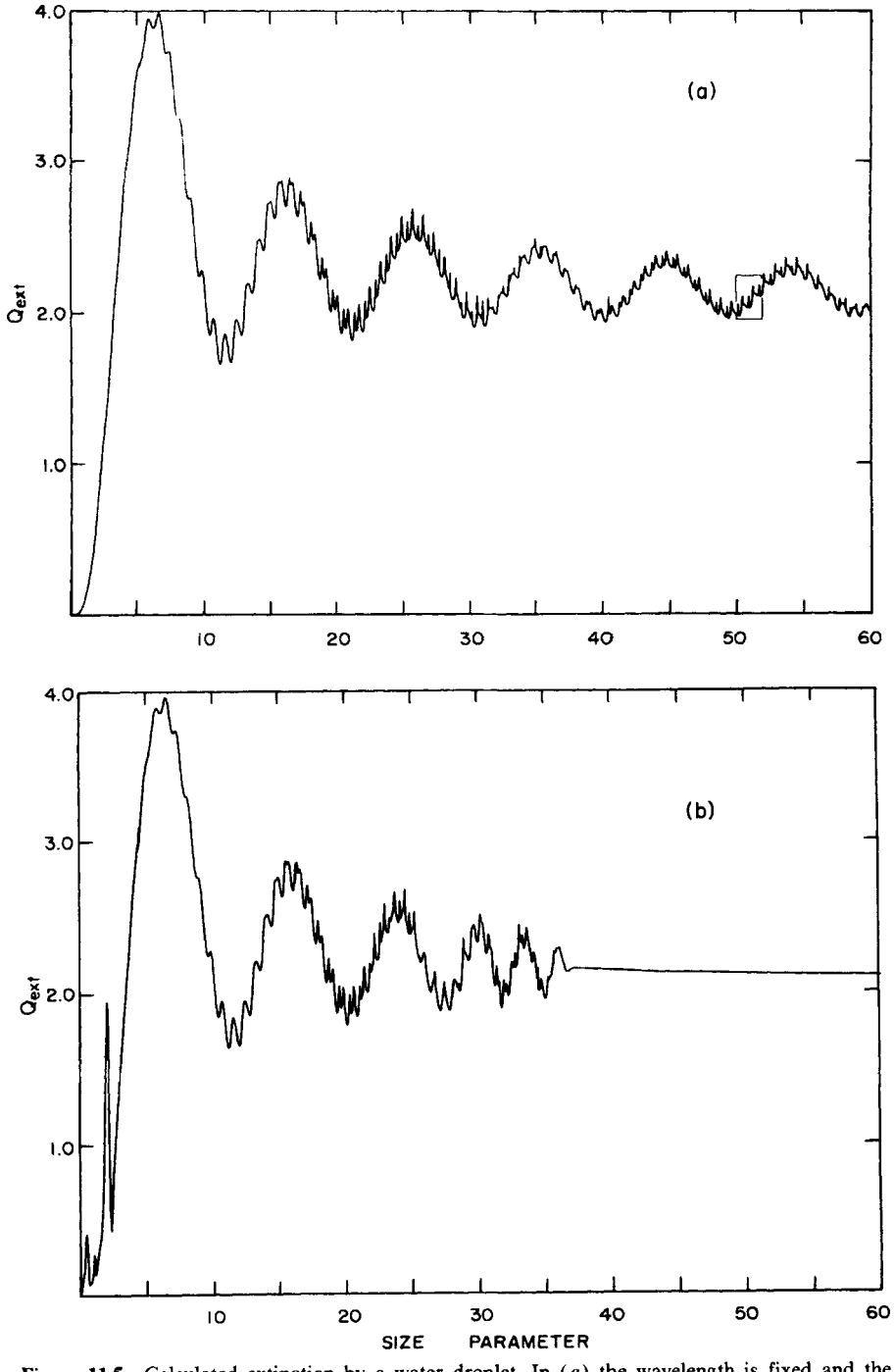

Figure 11.5 Calculated extinction by a water droplet. In (*a*) the wavelength is fixed and the radius is varied; in (*b*) the radius (1.0 μm) is fixed and the wavelength is varied.

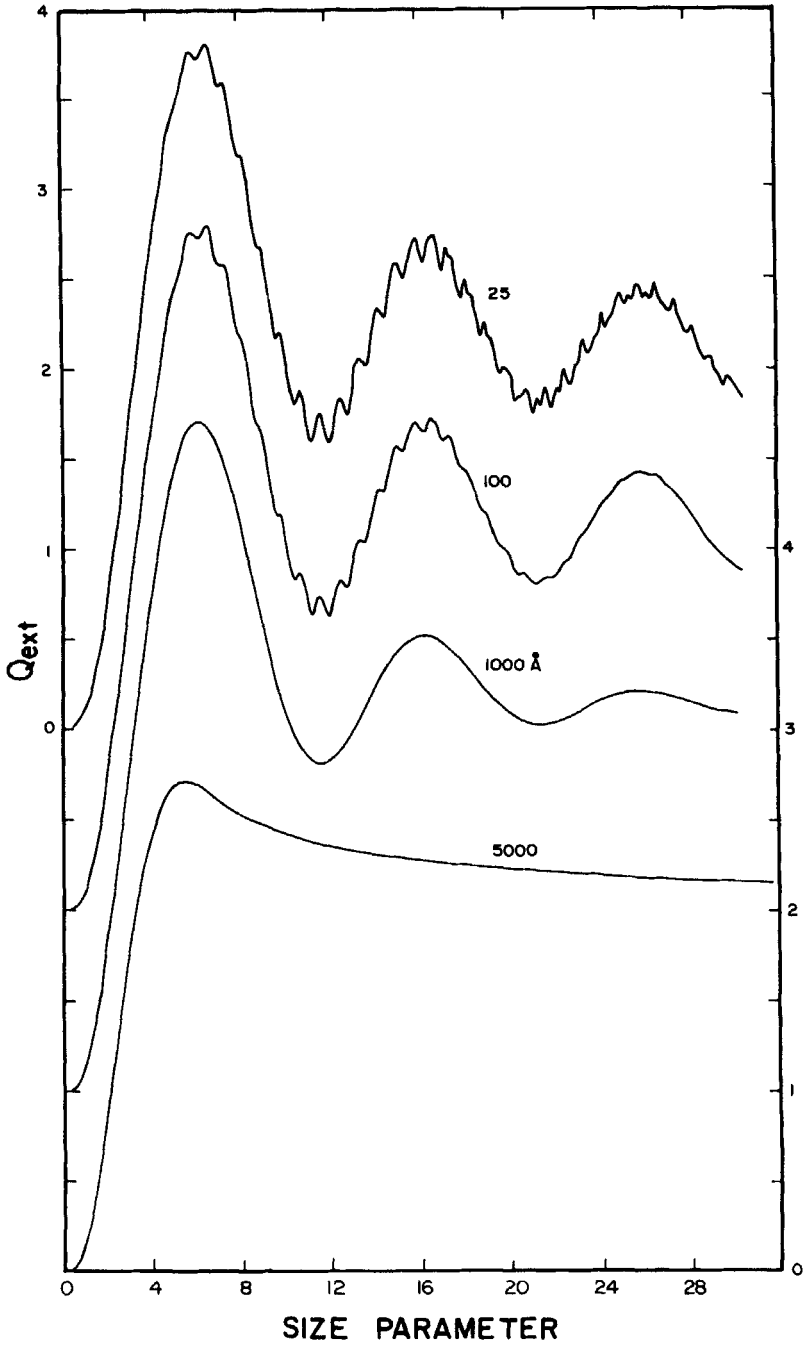

Figure 11.6 The effect of size dispersion on extinction of visible light by water droplets. Each curve is labeled with σ, the standard deviation in the Gaussian size distribution.

where $\bar{a}$ is the mean radius and σ^2 is the variance. Although the Gaussian distribution probably does not represent natural aerosols and other particulate systems very well its advantages are simplicity and familiarity.

To show the effect of increasing size dispersion on extinction a series of calculations for water droplets is given in Fig. 11.6. The topmost curve reproduces the calculations of Fig. 11.5*a* for a single sphere; the standard deviation σ is increased in successively lower curves.

Ripple structure, beginning with the sharpest at large size parameters, is the first to disappear as σ is increased. As the distribution is further widened, the interference structure fades away. For the widest distribution the only remaining features are reddening at small size parameters, and, at the other extreme, an asymptotic approach to the limiting value 2.

Without an appreciation for the possible spread of sizes in real particulate systems the values of σ in Fig. 11.6 are merely those of an adjustable parameter. We therefore give distribution widths for some natural and artificial aerosols and hydrosols in Table 11.1; we excluded from this list broad distributions, such as raindrops, to which the notion of a width is not really applicable.

Table 11.1 Approximate Size Distribution Parameters for Some Natural and Artificial Aerosols and Hydrosols

Particles	Mean Radius (μm)	Fractional Standard Deviation	Reference
Polystyrene spheres in water	0.05–2	0.005–0.01	
Bergland–Liu generator		0.01	Bergland and Liu (1973)
Sinclair–LaMer generator		0.1–0.2	Kerker (1969, p. 320)
Ultrasonic nebulizer		0.3	Perry et al. (1978)
Nozzles and sprays	20–300	1.1	Corn and Esmen (1976)
Corn rust spores	3.4	0.038	Corn and Esmen (1976)
Lycopodium spores	15	0.01	Corn and Esmen (1976)
Blood cells (dried)	8	0.08	Corn and Esmen (1976)
Clover pollen	26	0.04	Corn and Esmen (1976)
Giant ragweed pollen	9.8	0.05	Corn and Esmen (1976)
Orchard grass pollen	15.5	0.07	Corn and Esmen (1976)
Upper clouds of Venus	1.0	0.3	Hansen and Hovenier (1974)

11.4 RIPPLE STRUCTURE

Ripple structure—sharp, irregularly spaced features in extinction by weakly absorbing spheres—is evident in Figs. 4.6, 11.3, 11.5, and 11.6. In some ways ripple structure is merely a nuisance. It is, after all, unlikely to be observed in extinction by many polydispersions, natural and artificial. Yet calculations for a single sphere are of necessity done at a finite number of size parameters, one of which may just happen to correspond to a sharp peak unrepresentative of the generally smooth variation of extinction. Ways have been devised to get around this problem (see, e.g., Penndorf, 1958). Often the best approach in these days of fast computers is to do calculations for a distribution of sizes rather than for a single size (see Fig. 11.6). Before the digital computer was commonplace it was prohibitively expensive to do calculations for a very fine size parameter grid. Consequently, many of the older extinction curves do not exhibit as much structure as that shown in Fig. 11.5*a*. But even this curve is not indicative of the extreme fineness of extinction structure. A closer look at a small part of Fig. 11.5*a* (enclosed by a rectangle) reveals even more structure. Figure 11.7 shows results of extinction calculations for a water droplet similar to those of Chýlek et al. (1978a). Structure that was barely perceptible in Fig. 11.5*a* is now well resolved. Even on this expanded scale, however, there are unresolved extinction peaks; these are indicated by the vertical lines at about $x = 50.33$, 50.68, 51.12, and 51.90. To resolve these peaks requires an even finer size parameter grid. For example by decreasing Δx to 10^{-6} the peak near $x = 50.33$ is resolved in Fig. 11.8. Thus, the closer we look the more structure we find. One might well wonder if there is an end to this: is it a matter of dogs having fleas, which themselves have fleas, and so on *ad infinitum*? Chýlek et al. (1978a) have made a careful study of this question and claim that no more

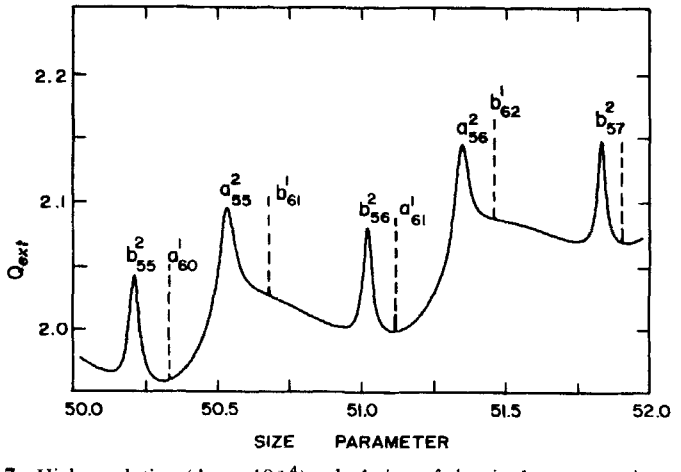

Figure 11.7 High-resolution ($\Delta x = 10^{-4}$) calculation of the ripple structure in extinction by a water droplet ($m = 1.33 + i10^{-8}$). After Chýlek et al. (1978a).

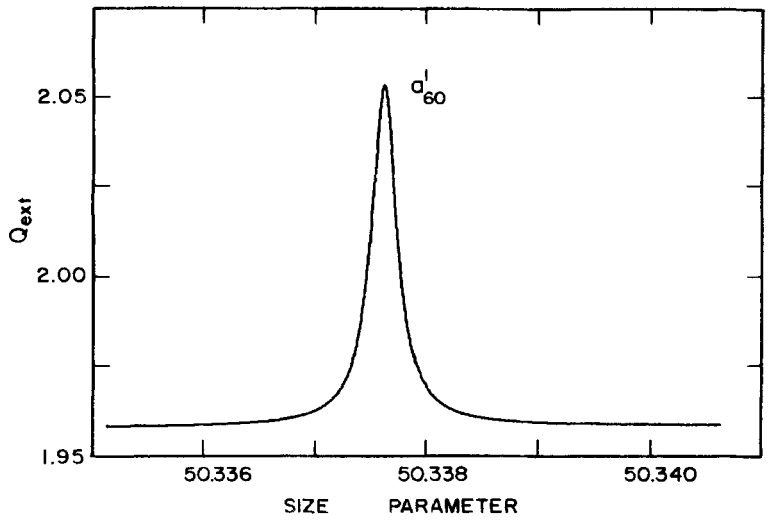

Figure 11.8 The unresolved extinction peak near $x = 50.33$ in Fig. 11.7 is resolved by decreasing Δx to 10^{-6}.

structure is revealed by decreasing Δx below 10^{-7}; therefore, the peak shown in Fig. 11.8 is an example of the narrowest to be found. Ripple structure is not limited to the scattering component of extinction but is present in absorption as well (Bennett and Rosasco, 1978).

We discussed in Section 4.3 the electromagnetic normal modes, or virtual modes, of a sphere, which are resonant when the denominators of the scattering coefficients a_n and b_n are minima (strictly speaking, when they vanish, but they only do so for complex frequencies or, equivalently, complex size parameters). But Q_{ext} is an infinite series in a_n and b_n, so ripple structure in extinction must be associated with these modes. The coefficient c_n (d_n) of the internal field has the same denominator as $b_n(a_n)$. Therefore, the energy density, and hence energy absorption, inside the sphere peaks at each resonance: there is ripple structure in absorption as well as scattering.

For each index n there is a sequence of values of x for which the mode associated with a_n or b_n is excited. We may therefore label each (nonoverlapping) extinction peak with the type of mode [electric (a_n) or magnetic (b_n)], the index n, and the sequential order of x (Chýlek, 1976): for example, a^1_{60}, a^2_{60}, and so on, where the superscript indicates the order of x; the extinction peaks between $x = 50$ and $x = 52$ for a water droplet are so labeled in Fig. 11.7.

Three peaks, labeled a^1_{60}, a^2_{60}, a^3_{60}, in the real part of $a_{60}(x)$ for a water droplet are shown in Fig. 11.9; the real part of the refractive index is fixed but the imaginary part is varied. These optical constants could be obtained by, for example, adding a little dye (food coloring) to water; this would increase k without appreciably changing n. Note that the horizontal scale is different for

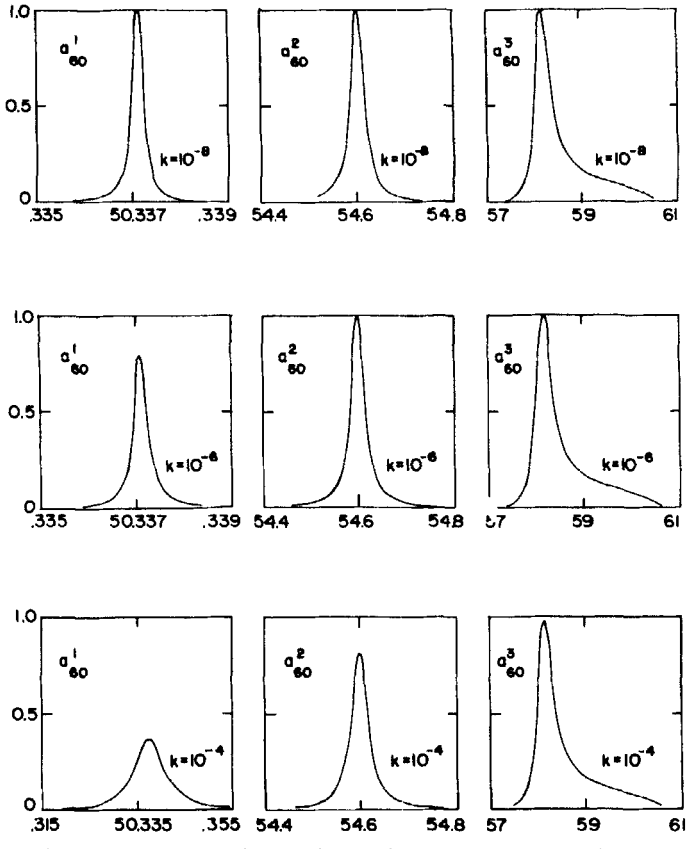

Figure 11.9 Three peaks in the real part of a_{60}. The imaginary part of the refractive index is progressively increased from top to bottom but the real part is fixed (1.33). After Chýlek et al. (1978b).

each set of curves. Similar curves, for different optical constants, have been given by Chýlek et al. (1978b).

The peaks appear to be Lorentzian, and if we were to plot $\mathrm{Im}\{a_{60}(x)\}$ this would be even more obvious. That this is indeed so, to good approximation, was shown by Fuchs and Kliewer (1968), who discussed in detail the normal modes of an ionic sphere.

For given k, the peaks broaden with increasing order. As absorption is increased for a fixed order each peak is broadened at the expense of its height, particularly the a_{60}^1 peak; the broader, higher-order peaks are not nearly as severely damped by absorption. This accounts for the rapid loss of the sharpest extinction peaks with increased absorption (Fig. 11.12).

Ripple structure was observed in scattering at 90° by water droplets as they nucleated and grew in a cloud chamber (Dobbins and Eklund, 1977). We shall show in Section 11.7 that ripple structure is easily observed in extinction by

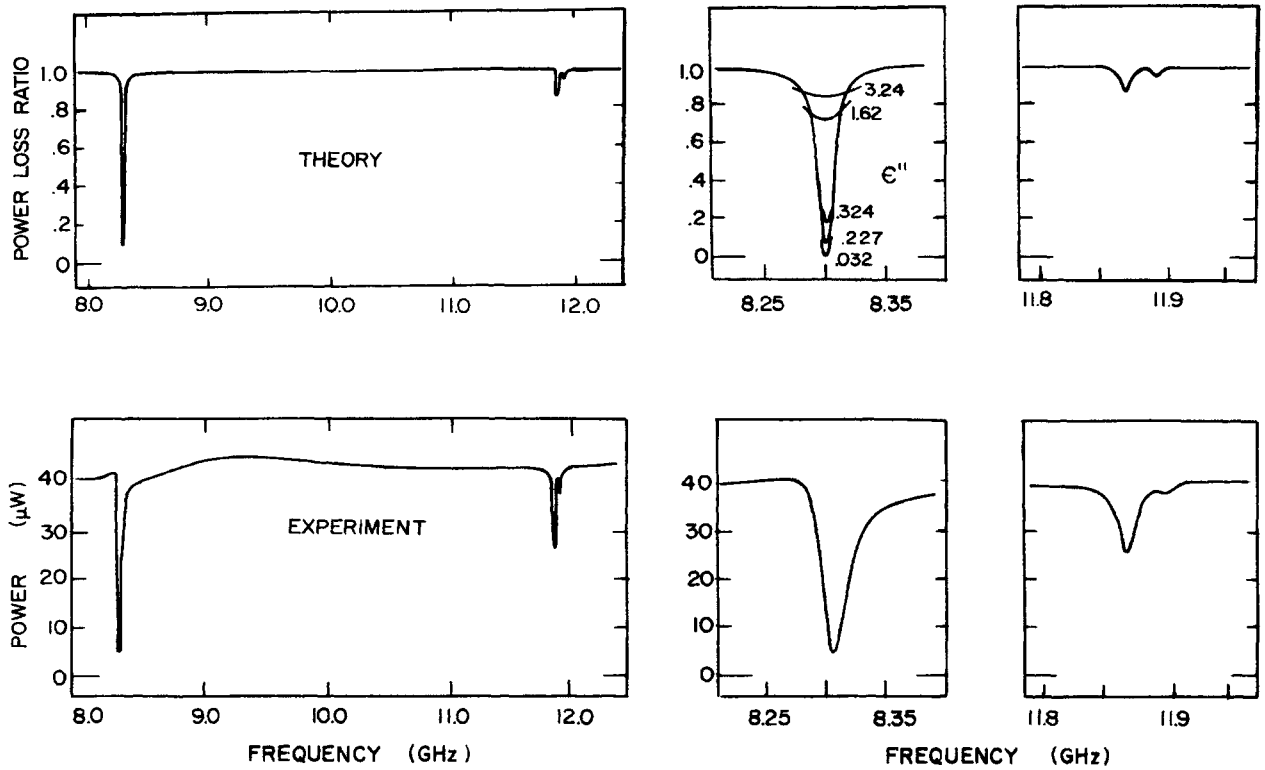

Figure 11.10 Theoretical power loss ratio for a sphere in a waveguide (upper curves) compared with measured transmission spectra (lower curves). The curves on the right are enlargements of the two bands; the effect of absorption on the lowest frequency band is shown in the upper right. From P. Affolter and B. Eliasson, *IEEE Trans. Microwave Theory Tech.*, **MTT-21** (1973), 573–578; © 1973 IEEE.

polystyrene spheres suspended in water. In both these examples the ripples are fairly broad and therefore can be observed despite the distribution of particle sizes. Single spheres are required, however, if one is to observe the very sharp structure associated with larger, more refractive spheres. Such observations have been reported for the microwave and visible regions; these are discussed below.

11.4.1 Sphere in a Microwave Waveguide

The possibility of making use of ripple structure in microwave devices has been discussed for years (e.g., Richtmyer, 1939). For example, a "notch" filter can be made by combining a sphere with a waveguide. This was done by Affolter and Eliasson (1973): they suspended a 0.2-cm $SrTiO_3$ ($\epsilon' = 324.4$) sphere symmetrically in a waveguide and measured the transmitted power as a function of frequency. Their results are shown in the lower part of Fig. 11.10; calculations of the power loss ratio (equivalent to I/I_0 in our notation) are shown in the upper part of this figure. Attenuation of microwave power is almost complete in a narrow frequency band. Calculations show that the shape of this band strongly depends on ϵ'', which is also evident in Fig. 11.12; Affolter and Eliasson suggested that this could be used to measure ϵ'' of weakly absorbing materials.

11.4.2 Ripples in Radiation Pressure

It might be thought that ripple structure, particularly the sharp features at large x (Fig. 11.5), would be primarily of theoretical interest because it could not be observed in a distribution of sizes. Even with a single particle a small dispersion of wavelengths would obliterate such structure. In recent years, however, many features of the complex ripple structure pattern have been observed in a set of elegant and beautiful experiments. Ashkin and Dziedzic (1971, 1976, 1977) have developed a method of levitating transparent particles in a strongly focused laser beam. Not only is a particle balanced against gravity by radiation pressure, it is also laterally stabilized in the beam. An electronic feedback system adjusts the laser power so that a particle is kept at a fixed height. If the wavelength is varied, then the radiation pressure, and hence the laser power necessary for stable levitation, also varies; this technique has been called radiation-pressure-force spectroscopy.

The power required to levitate an oil drop as its size parameter is varied by tuning the dye laser wavelength is shown in the lower curves of Fig. 11.11. The calculated radiation pressure efficiency (plotted as $1/Q_{pr}$) is shown in the middle curve and Q_{ext} in the upper curve; the refractive index $m = 1.47 + i10^{-6}$ is approximately constant over the small wavelength interval. This figure is taken from Chýlek et al. (1978b), who identified the peaks in the upper curve. Curve a of the experimental results is for values of x calculated from the drop size determined microscopically with an accuracy of $\pm 5\%$. The ripple structure

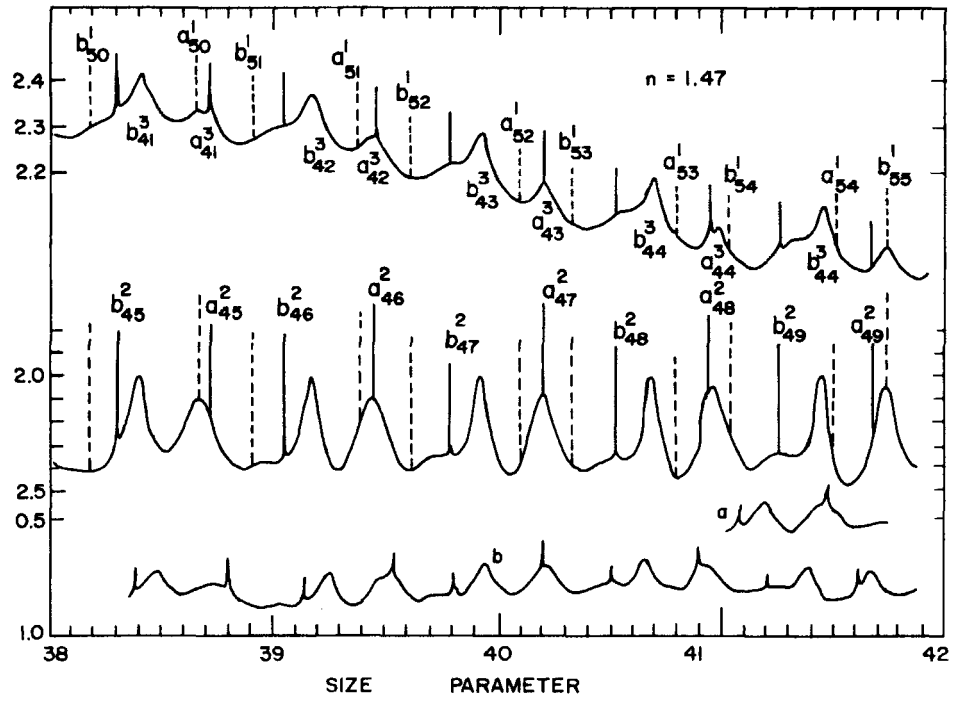

Figure 11.11 Calculated extinction and radiation pressure for a sphere compared with the power necessary to levitate the sphere. From Chýlek et al. (1978b), who used the experimental results of Ashkin and Dziedzic (1977).

features are so distinctive, however, that a much more accurate determination of x was made by matching experimental and theoretical curves; curve b is based on the more accurate drop size. Experiment and theory now agree very well except for the small displacements attributed to drop evaporation during the scan. All features of the calculated spectrum are observed in the measurements except those with width Δx of order 10^{-6}, shown as dashed lines in the calculations. These correspond to first-order resonances of the normal modes (e.g., b_{50}^{1}, a_{52}^{1}, etc.) and are too narrow to be resolved despite the laser's high spectral purity.

The experiments of Ashkin and Dziedzic impressively demonstrate the complexity of the electromagnetic modes of a sphere and the high degree of accuracy with which Mie theory describes them; they also provide a means for measuring the sizes of single spheres to within 1 part in 10^5 or 10^6 and for sensitively monitoring small size changes.

11.5 ABSORPTION EFFECTS IN EXTINCTION

At this point the reader should be well aware that all solids and liquids are strongly absorbing in some spectral regions and that this has consequences for

extinction, some of which were discussed in the survey section (11.1). We examine the effects of absorption on extinction further in this section.

11.5.1 Ripple and Interference Structure

Absorption is progressively increased in the sequence of extinction curves in Fig. 11.12 for a narrow Gaussian distribution of radii. Because the refractive index (wavelength) is fixed for each curve the abscissa is proportional to the mean radius. Although the optical constants for the upper curves are similar to those of water at some infrared wavelengths, $m = 1.33 + i0.1$ is not; in this particular instance our point is better made by varying only k despite our general aversion to this sort of arbitrary and unrealistic fiddling with optical constants.

It is obvious at a glance that ripple structure is the first to fade as absorption is increased, beginning at the larger values of x. Next, the interference structure is damped, and again, it is more pronounced for large x. In Section 4.4 we interpreted this structure as arising from interference between the undeviated beam and the central ray through a sphere. Consistent with this interpretation is the expectation that these extrema should vanish whenever k is sufficiently large ($kx > 1$) that no appreciable light penetrates through the particle; that this is so is evident from Fig. 11.12.

11.5.2 Effect of an Absorption Edge

What is at first sight a paradox emerges from careful study of Fig. 11.12: extinction at fixed x does not always increase with increasing k. For example, at $x = 2$ extinction increases with increasing absorption; this is most evident in the bottom two curves. But at $x = 6$ it decreases with increasing absorption. At $x = 11$, however, there is again a reversal. Thus, the effect of a rapid onset of strong absorption, such as that occurring in the ultraviolet for all insulating solids and liquids, will depend on the particle size. For example, near the absorption edge of MgO (~ 7 eV) extinction by a 0.01-μm sphere sharply increases (Fig. 11.2). But when the radius is increased to 0.05 μm, extinction sharply drops just beyond the absorption edge. These effects are more clearly apparent in the experimental extinction curves for polystyrene (Fig. 11.19). The physical reason why increasing absorption can decrease extinction is that interference is thwarted if the light does not penetrate through the particle. At size parameters corresponding to interference peaks—destructive interference—an absorption edge decreases extinction; conversely, at size parameters corresponding to interference valleys, thwarting of constructive interference increases extinction.

11.5.3 Asymmetry Associated with Narrow Absorption Bands

Suppose that a material has a narrow, symmetric absorption band in the bulk state. It seems no more than common sense to expect that the corresponding

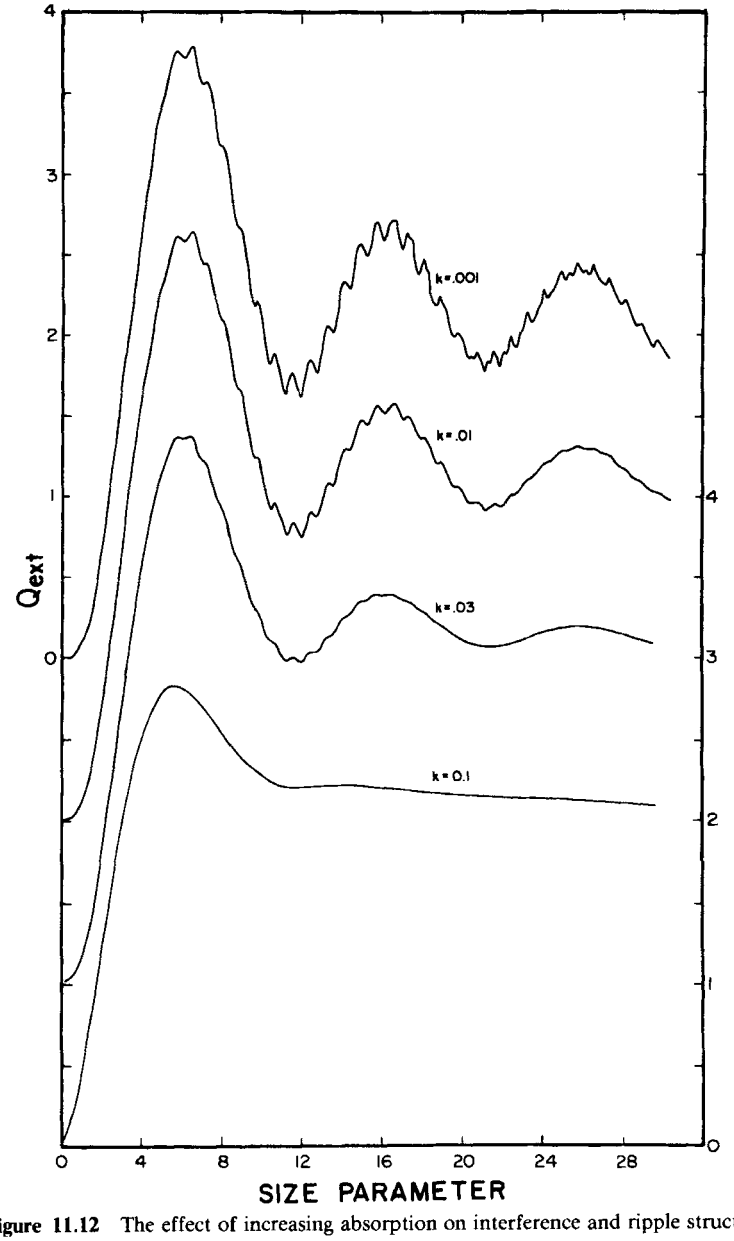

Figure 11.12 The effect of increasing absorption on interference and ripple structure.

extinction band for a particle of this material should also be symmetric. Yet when the particle is sufficiently large that the extinction band has an appreciable scattering component, it may be not at all symmetric. This type of asymmetry was first pointed out by van de Hulst (1957) in connection with small particles of the interstellar medium. Since then various calculations have been made for both coated and uncoated particles (Wickramasinghe and

Nandy, 1970; Greenberg and Stoeckly, 1971; Greenberg and Hong, 1974).

We have chosen the sharp absorption band at 1.18 eV in radiation-damaged MgO (see the inset curves in Figs. 10.1 and 11.2) to illustrate the asymmetry effect. The band strength derived from measurements is not sufficient to clearly illustrate the effect, so we increased it, along with the strengths of the three broader peaks that accompany it, by a factor of 100. Optical constants were calculated from the multioscillator model (9.25) with parameters chosen to best fit the data; then the strengths ω_{pj}^2 were increased a hundredfold. The resulting band strengths might be thought of as representing much higher levels of radiation damage, although it is doubtful that they could be realized in this way. The maximum ϵ'' of the enhanced 1.18-eV band is 0.082, corresponding to a k of about 0.024. Note that this is still some hundreds of times lower than intrinsic absorption in MgO between 7 and 20 eV.

Calculations for a range of particle sizes are shown in Fig. 11.13. Note that the scales have not been shifted for the different sizes: extinction increases with size because of scattering. The extinction band for the 0.1-μm particle faithfully reflects the characteristics of the intrinsic absorption band. But asymmetries develop for particles larger than about 0.2 μm; indeed, at a radius of 0.3 μm the absorption band looks like an "emission" band relative to the continuum. The explanation for this strange extinction behavior near an absorption band lies in the preceding section: extinction is not a steadily increasing function of bulk absorption. A narrow absorption band is similar to a small absorption edge that falls just as rapidly as it rises, which can thus cause extinction peaks, dips, or both.

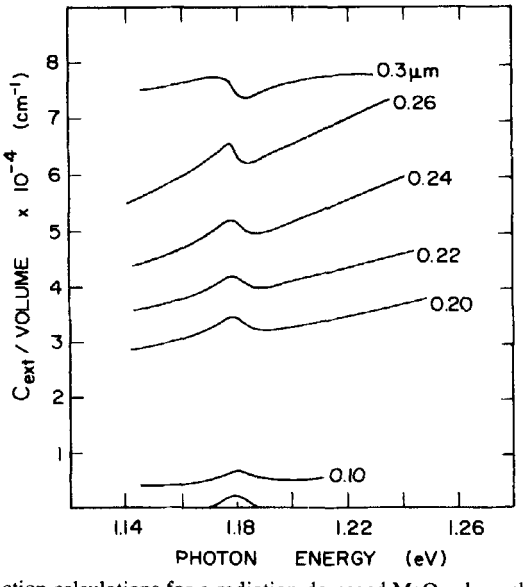

Figure 11.13 Extinction calculations for a radiation-damaged MgO sphere showing how increasing size gives asymmetric bands. The lowest curve (unlabeled) is for a sphere of radius 0.01 μm. From Huffman (1977).

11.5.4 Dominance of Absorption in the Rayleigh Limit

Extinction is proportional to the square of the volume of a particle small compared with the wavelength—but only if absorption is negligible. If it is not it will always dominate over scattering for sufficiently small sizes [see (5.12)], in which instance extinction is proportional to particle volume. The volume attenuation coefficient $\alpha_v = C_{ext}/v$ of water droplets is shown as a function of radius in Fig. 11.14*a* for a set of wavelengths. Water is very weakly absorbing at visible wavelengths ($k < 10^{-8}$) and extinction is therefore dominated by scattering; interference structure is evident but ripple structure has been suppressed for clarity. As the wavelength is increased the first interference peak shifts to larger radii; and α_v is constant for the smaller sizes, which indicates that extinction is predominantly absorption. At wavelengths where absorption is sufficiently strong (e.g., $\lambda = 12.5$ μm) α_v is constant until the radius is so large that almost no light penetrates into the particle's interior; this has practical consequences: at such wavelengths extinction by a polydispersion is independent of the details of the size distribution provided that the volume fraction of larger particles is small. Thus, Carlon et al. (1977) suggested that liquid water content along a path in the atmosphere could be determined by measuring attenuation of an infrared beam along that path. Most solids and liquids are somewhat absorbing in the infrared; moreover, larger particles have short atmospheric residence times. So extinction of infrared radiation by atmospheric aerosols is expected to be nearly independent of size (but not necessarily shape, as we shall see in Chapter 12), and attenuation measurements could therefore be used to remotely monitor their total volume.

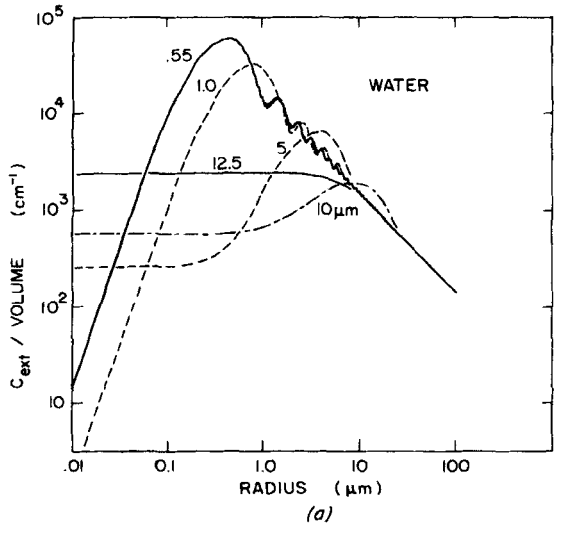

Figure 11.14 Volume-normalized extinction as a function of size calculated for spheres of (*a*) water (after Carlon et al., 1977) and (*b*) aluminum (from Rathmann, 1981). The optical constants used are those appropriate to the wavelengths noted on the curves.

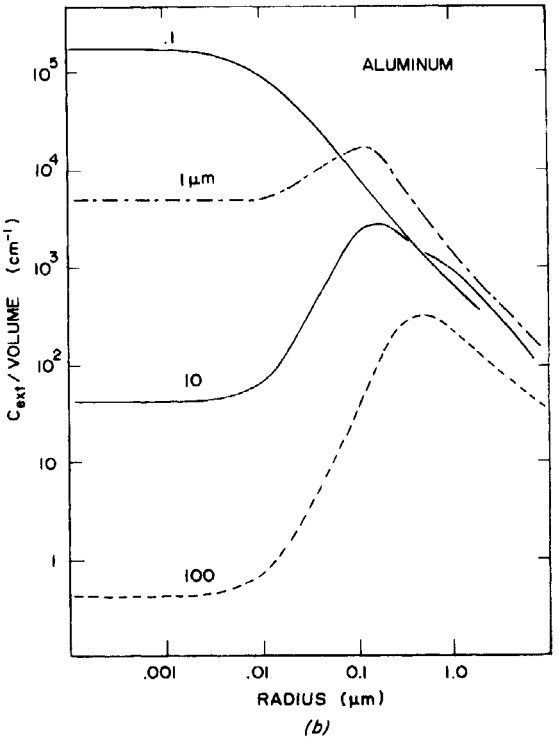

Figure 11.14 (*Continued*)

There are some notable differences apparent in Fig. 11.14 between the extinction curves for aluminum spheres and those for water droplets. For example, α_v is still constant for sufficiently small aluminum particles but the range of sizes is more restricted. The large peak is *not* an interference maximum: aluminum is too absorbing for that. Rather it is the dominance of the magnetic dipole term b_1 in the series (4.62). Physically, this absorption arises from eddy current losses, which are strong when the particle size is near, but less than, the skin depth. At $\lambda = 0.1$ μm the skin depth is less than the radius, so the interior of the particle is shielded from the field; eddy current losses are confined to the vicinity of the surface and therefore the volume of absorbing material is reduced.

11.6 EXTINCTION CALCULATIONS FOR NONSPHERICAL PARTICLES

To this point we have dealt only with spheres, which have the advantage that their extinction properties are easily calculated while still giving substantial guidance into extinction by small particles in general. And there are many particles that are indeed spherical: cloud droplets; sulfuric acid droplets

(apparently present in the upper clouds of Venus); sulfur colloids; and the much-used polystyrene spheres. For such particles Mie theory is admirably suited.

A few particles, such as spores, seem to be rather well approximated by spheroids, and there are many examples of elongated particles which may fairly well be described as infinite cylinders. Our next step toward understanding extinction by nonspherical particles is to consider calculations for these two shapes. To a limited extent this has already been done: spheroids small compared with the wavelength in Chapter 5 and normally illuminated cylinders in Chapter 8. We remove these restrictions in this section; measurements are presented in the following section. Because calculations for these shapes are more difficult than for spheres, we shall rely heavily on those of others.

11.6.1 Spheroids

Asano and Yamamoto (1975) solved the problem of absorption and scattering by an isotropic, homogeneous spheroid of arbitrary size by expanding the fields in vector spheroidal harmonics and determining the coefficients of the scattered field in a manner similar to that for a sphere (Chapter 4). A few results of calculations were given in this first paper; Asano (1979) subsequently published a more extensive set of calculations of scattering and absorption by spheroids of varying size, shape, and refractive index under various conditions of illumination. We now borrow a few examples from this work to extend our understanding of extinction by nonspherical particles. We note immediately that three factors add complications beyond those for spheres. First, a spheroid may be either prolate or oblate; second, the direction and state of polarization of the incident beam must be specified; and third, a spheroid has two characteristic lengths, its major and minor axes. As a consequence, the number of possible sets of calculations in a complete treatment of extinction by spheroids is vastly greater than that for spheres. Out of this multitude we have chosen only a few for illustration.

Figure 11.15 shows Asano's calculations of extinction by nonabsorbing spheroids for an incident beam parallel to the symmetry axis, which is the major axis for prolate and the minor axis for oblate spheroids. Because of axial symmetry extinction in this instance is independent of polarization. Calculations of the scattering efficiency Q_{sca}, defined as the scattering cross section divided by the particle's cross-sectional area projected onto a plane normal to the incident beam, are shown for various degrees of elongation specified by the ratio of the major to minor axes (a/b); the size parameter $x = 2\pi a/\lambda$ is determined by the semimajor axis a.

A glance at the curves in Fig. 11.15 reveals extinction characteristics similar to those for spheres: at small size parameters there is a Rayleigh-like increase of Q_{sca} with x followed by an approximately linear region; broad-scale interference structure is evident as is finer ripple structure, particularly in the curves for the oblate spheroids. The interference structure can be explained

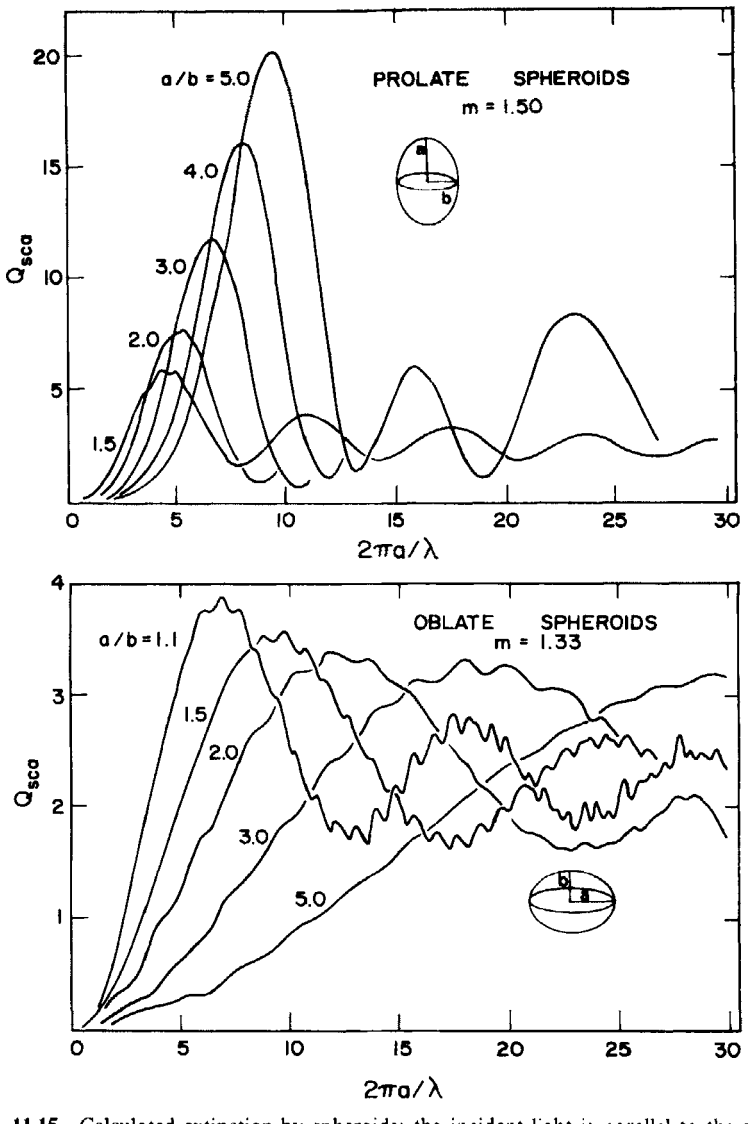

Figure 11.15 Calculated extinction by spheroids; the incident light is parallel to the symmetry axis. From Asano (1979).

qualitatively, as was done for spheres in Section 4.4, as alternate destructive and constructive interference between the ray passing through the center of the particle, thereby undergoing a phase shift of $4\pi a(m - 1)/\lambda$, and the undeviated beam. For the prolate spheroids, with $m = 1.5$, this phase shift is simply x, and we might expect the positions of the extinction maxima to be independent of elongation. This does not, however, occur, although the separation Δx

between peaks is approximately 2π. Note in particular that the position of the first extinction maximum (the first destructive interference) shifts to larger x with increasing elongation a/b. Asano has attributed this to edge phenomena, which become more important as the curvature at the point where the incident beam grazes the particle decreases, that is, with increasing a/b (for fixed a). In the limit $a/b \to \infty$ the prolate spheroid illuminated end on becomes an infinite cylinder with the wave propagating along its axis (i.e., a cylindrical waveguide); there is indeed some similarity between the extinction curve in Fig. 11.15 for the largest a/b and that for an infinite cylinder illuminated at nearly grazing incidence (Fig. 11.17). Additional evidence in support of this interpretation is provided by the curves in Fig. 11.15 for oblate spheroids; the curvature of such spheroids at the point of grazing *increases* with increasing a/b (for fixed a). If we were to plot Q_{sca} for the oblate spheroids as a function of the phase shift parameter $4\pi b(m - 1)/\lambda$, the positions of the first maxima would be more nearly congruent than they were for the prolate spheroids.

Perhaps the greatest difference between the extinction calculations for prolate and oblate spheroids is in the ripple structure, which is much more obvious for the latter and even persists to the largest a/b ratios shown, although with reduced amplitude.

Asano's calculations of absorption and scattering efficiencies for an absorbing prolate spheroid (which are not reproduced here) are qualitatively similar to those for spheres. For example, absorption dampens both large- and small-scale oscillations. As x increases Q_{abs} and Q_{sca} approach the respective asymptotic limits $1 - Q_{refl}$ and $1 + Q_{refl}$; Q_{refl}, the average reflectance over the particle's illuminated face (see Section 7.1), is small for the given refractive index $(1.5 + i0.1)$, so in this instance the asymptotic efficiencies are approximately 1. The extinction efficiency therefore oscillates about two with decreasing amplitude as x increases.

Extinction calculations for obliquely incident light, also taken from Asano (1979), are shown in Fig. 11.16. The symmetry axis is parallel to the z axis and the direction of the incident beam, which makes an angle ζ with the symmetry axis, lies in the xz plane, the plane of incidence. The incident light is polarized either with its electric field or its magnetic field perpendicular to the plane of incidence; these two polarization states are denoted by TE (transverse electric) and TM (transverse magnetic).

Straight lines connect the extinction efficiencies computed at size parameter intervals $\Delta x = 1$; this coarse spacing attests to the difficulties of doing computations for obliquely incident light. In general, TE and TM waves are scattered similarly, although there are slight differences which lead to polarization (in the forward direction) of unpolarized obliquely incident light. Extinction of light incident along the symmetry axis of the oblate spheroid is broad and rippled, but the maximum becomes more peaked and shifts to smaller values of x as the obliquity is increased (i.e., as ζ is increased from 0° to 90°). For the prolate spheroid a similar, but opposite, effect is evident: the first extinction maximum decreases and shifts to larger values of x with increasing

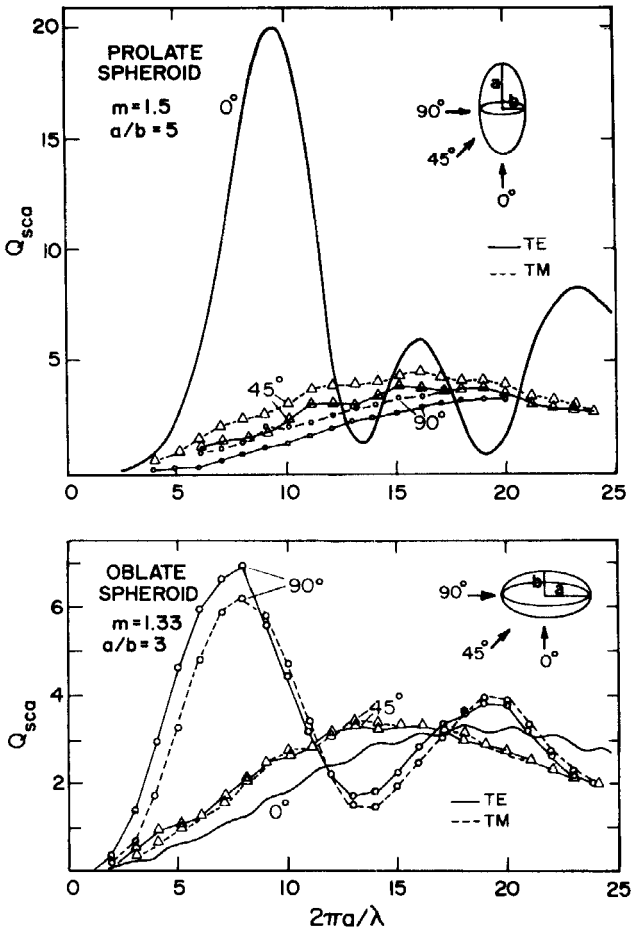

Figure 11.16 Calculated extinction of obliquely incident light by spheroids. From Asano (1979).

obliquity. It should be kept in mind, however, in interpreting these results that the distance through the center of the prolate spheroid *along the direction of incidence* decreases with increasing obliquity, whereas the opposite is true for the oblate spheroid. Extinction by the prolate spheroid, which is rather elongated ($a/b = 5$), is quite similar to that by an infinite cylinder, which we discuss next.

11.6.2 Infinite Cylinder

An infinite right circular cylinder is another particle shape for which the scattering problem is exactly soluble (Section 8.4), although it might be thought that such cylinders are so unphysical as to be totally irrelevant to real

problems. But microwave extinction measurements (discussed in Section 11.7) indicate that finite cylinders with length-to-diameter ratios as low as about 5 can be closely approximated as infinite cylinders. Thus, many problems involving particles such as textile fibers, asbestos fibers, and even smoke particles aggregated into chain-like structures, can be treated adequately within the framework of infinite cylinder theory.

We have already given examples of extinction by infinite cylinders illuminated normally to their axes (Section 8.4), and Appendix C contains a

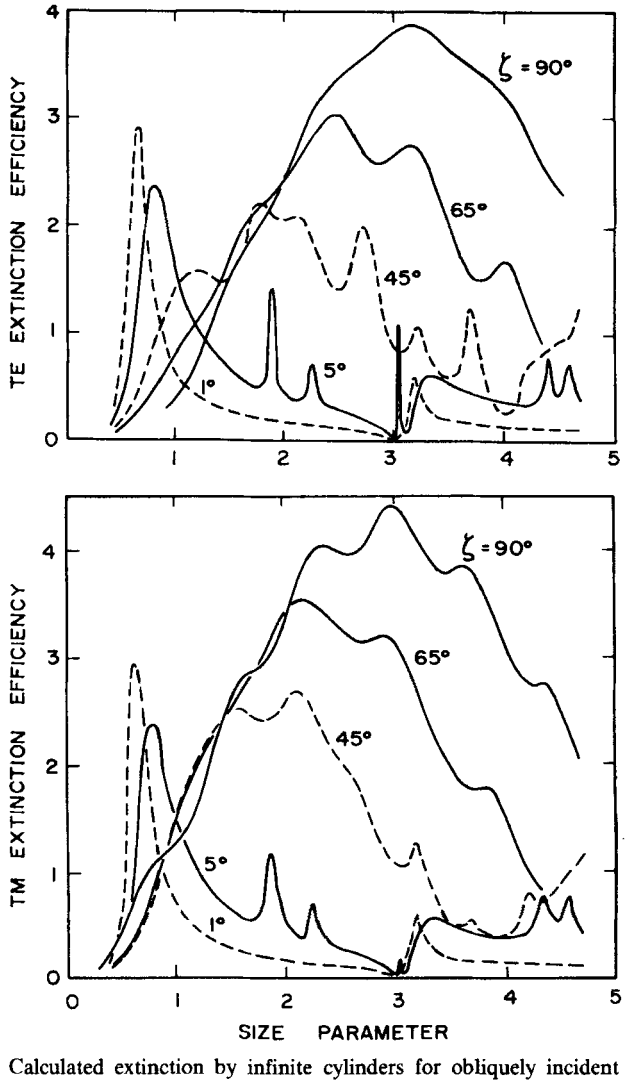

Figure 11.17 Calculated extinction by infinite cylinders for obliquely incident light; $\zeta = 90°$ corresponds to normally incident light. TE and TM denote light with the electric and magnetic vectors, respectively, perpendicular to the xz plane. From Lind and Greenberg (1966).

program for such computations. The same type of computations are required to determine extinction of obliquely incident light; although we omit the details here, they may be found in the paper by Lind and Greenberg (1966), from which we have taken Fig. 11.17. The refractive index $m = 1.6$ is appropriate to Lucite at microwave frequencies. As the angle of incidence ζ is varied from 90° (normal) to 1° (nearly grazing), the extinction efficiencies for TE and TM waves approach each other, as required by symmetry. The curve of extinction as a function of size is broad and rippled when the light is normally incident but narrows as ζ is increased until at nearly grazing incidence it is a series of sharp peaks dominated by the one at smallest x; this was also evident in the extinction curves for the elongated prolate spheroid (Fig. 11.16). At grazing incidence the efficiencies vanish, but in this instance the cylinder is more properly considered as a waveguide.

It seems fairly obvious from inspection of Fig. 11.17 that the extinction curve for a collection of randomly oriented cylinders would be similar to that for a polydispersion of spheres.

11.7 EXTINCTION MEASUREMENTS

Extinction is determined by measuring the ratio of transmitted to incident irradiance (11.1). Many laboratories are equipped with recording spectrophotometers which can measure this quantity very quickly for liquid or solid samples. In principle this same type of instrument may be used for measuring extinction by particulate samples. The results, however, may be unreliable unless the detector is designed to reject forward-scattered light, which may be the major contributor to extinction by particles larger than the wavelength.

The essentials of a proper experimental arrangement for measuring extinction are shown in Fig. 11.18. Light from a point source is collimated by, for example, a lens, transmitted through the particulate sample, and focused through a small pinhole onto a detector. In principle, light scattered in other than the forward direction is not detected. Of course, the pinhole cannot be infinitesimally small; in practice, therefore, the acceptance angle is determined by the size of the pinhole and the focal length of the second lens. Figure 11.18 is only schematic, however; the effective size of the source may be reduced by additional apertures and a monochromator may be inserted in the system.

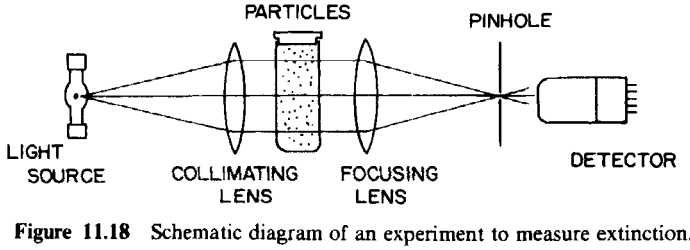

Figure 11.18 Schematic diagram of an experiment to measure extinction.

Although conventional spectrophotometers are not usually designed to reject light scattered at small angles, such instruments may be adequate for extinction measurements if the particles are not too large. But it is well to be aware of the potential pitfalls of measuring extinction this way. Several of the extinction curves in Chapter 12 for very small smoke particles ($< 0.1\ \mu m$) were obtained with a commercial spectrophotometer. Infrared scattering by such particles is small and nearly uniform in all directions, even for rather large refractive indices. In this instance the simple measurement technique is quite accurate.

11.7.1 Polystyrene Spheres

Measured extinction spectra for aqueous suspensions of polystyrene spheres—the light scatterer's old friend—are shown in Fig. 11.19. Water is transparent only between about 0.2 and 1.3 μm, which limits measurements to this interval. These curves were obtained with a Cary 14R spectrophotometer, a commonly available double-beam instrument which automatically adjusts for changing light intensity during a wavelength scan and plots a continuous, high-resolution curve of optical density. To reproduce the fine structure faithfully, the curves were traced exactly as they were plotted by the instru-

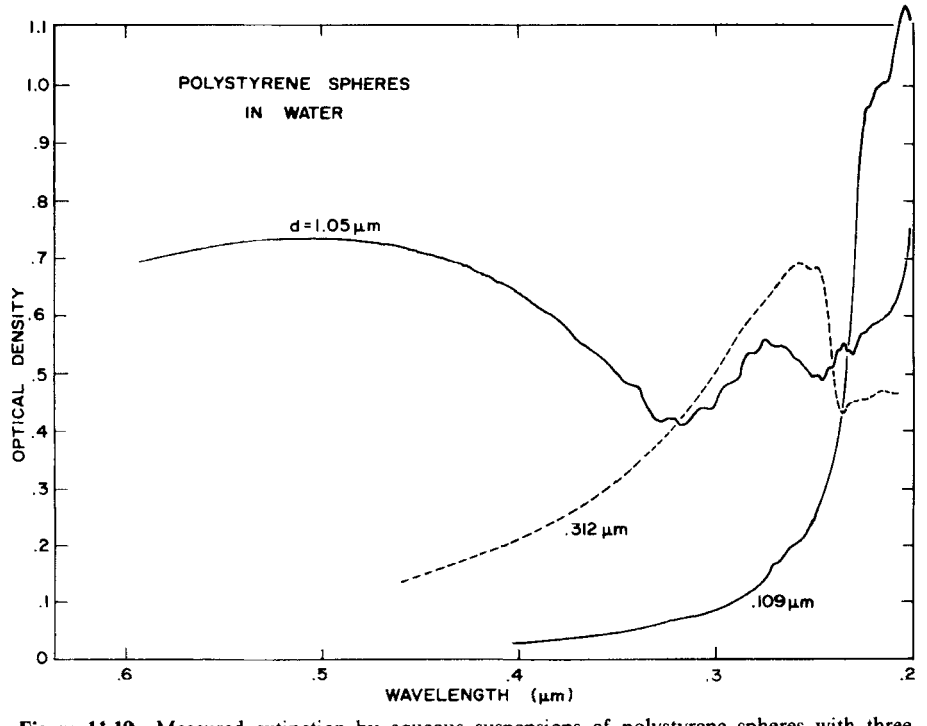

Figure 11.19 Measured extinction by aqueous suspensions of polystyrene spheres with three different mean diameters.

ment. Note that in contrast with previous extinction curves wavelength is the abscissa in Fig. 11.19. Although the measurements were not made using the "proper" experimental arrangement shown in Fig. 11.18, the particles are not too large and are suspended in water, so measured extinction is not greatly different from what would be obtained if forward-scattered light were excluded from the detector.

Almost all the calculated extinction features discussed previously may be found in the measured extinction curves: reddening when a/λ is small; interference peaks, the first of which shifts to longer wavelengths with increasing size; ripple structure; and the effects of an ultraviolet absorption edge. Reddening, as a result of greater scattering of shorter wavelengths, is evident in the spectrum for the 0.312-μm spheres. But the 1.05-μm spheres exhibit a tendency toward bluing, which is rare in natural aerosols. Even small-scale ripple structure, which sets in on the short-wavelength side of the interference peak for the 1.05-μm spheres, is obvious. Although such ripple structure is not usually observed in extinction spectra of polydispersions, it is in this instance because of the small size dispersion ($\sim$ 1%) and the high resolution of the spectrophotometer. Absorption dominates extinction by the smallest spheres and rises sharply near $\lambda = 0.23$ μm, the absorption edge of polystyrene; the barely perceptible features near 0.22 μm and 0.27 μm are also observed in bulk polystyrene (Inagaki et al., 1977). With the absorption edge so clearly marked it is apparent that the extinction band near 0.26 μm for the 0.312-μm spheres is a result of abrupt suppression of the first interference peak by strong absorption; this is an excellent experimental example of an effect that was discussed in Section 11.2 in connection with calculations for MgO and in Section 11.5.

Extinction spectra could be used to size particles by matching measured features with those calculated from Mie theory provided that the size distribution is narrow and the particles are nearly spherical.

11.7.2 Irregular Quartz Particles

Disappearance of prominent extinction features for spheres with an increase in the spread of sizes was illustrated in Fig. 11.6; similar effects occur for irregular particles. For example, Fig. 11.20 shows measurements for various size-graded fractions of irregularly shaped quartz particles suspended in water (Hodkinson, 1963). Measurements were made at three different wavelengths and the results plotted against size parameter (the refractive index changes only slightly). Data were normalized by assuming that the constant extinction efficiency at the largest size parameters was equal to the asymptotic limit 2. None of the prominent features calculated for spheres appear in these results; extinction merely rises steadily at small size parameters (reddening) to a constant value at large size parameters. Although some size information is present near values of x where extinction levels off it seems that accurate sizing of such a distribution of irregular particles by extinction holds little promise of success.

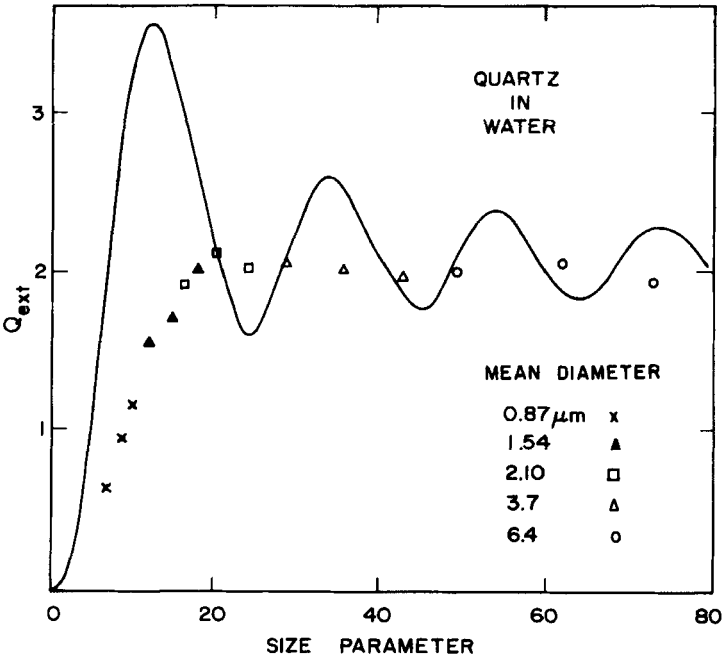

Figure 11.20 Measured extinction by five aqueous suspensions of irregular quartz particles (Hodkinson, 1963) at the wavelengths 0.365, 0.436, and 0.546 μm.

11.7.3 Additional Measurements

The measurements presented in the preceding two sections represent extremes: a highly monodisperse suspension of spheres with much extinction structure, and a broad size distribution of irregularly shaped particles with no prominent features. Measured extinction intermediate between these two extremes has been reported. For example, DeVore and Pfund (1947) segregated different size fractions of several fine powders on glass substrates. The first extinction maximum was clearly apparent for each sample, in contrast with the results in Fig. 11.20. These authors were even able to infer refractive indices of the powder solids by noting the shift of the first interference peak as the particles were surrounded by different liquids. Procter and Barker (1974) and Procter and Harris (1974) determined extinction by segregated size fractions of quartz and diamond dust. For these irregular particles there was evidence of the first interference maximum, after which extinction fell steadily toward the asymptotic limit.

11.7.4 Direct Measurement of Absorption

Extinction is not difficult to measure—in principle. But if it is to be separated into its components an independent measurement of either scattering or

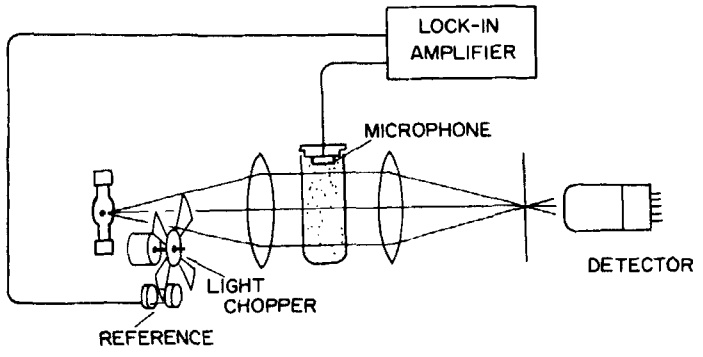

Figure 11.21 Schematic diagram of an experiment to measure absorption (using the photoacoustic method) and extinction.

absorption is required, which may be difficult. To determine total scattering either differential scattering measurements must be integrated over all directions or some special optical arrangement, such as an integrating sphere, must be used to collect all the scattered light. Errors in Q_{sca} are carried over into Q_{abs} inferred from $Q_{ext} - Q_{sca}$; and if $Q_{sca} \simeq Q_{ext}$ the relative error in Q_{abs} can be quite large. It is possible, however, to measure absorption directly—rather than extinction less scattering—by a method variously referred to as optoacoustic, photoacoustic, or spectrophone. Particles illuminated by light chopped at audio frequencies are periodically heated; this causes pressure oscillations (sound) which are detected by a sensitive microphone. Only absorbed light contributes to the heating, so absorption can be measured directly even in the presence of appreciable scattering. A schematic arrangement for simultaneously measuring absorption by the photoacoustic method and extinction is shown in Fig. 11.21. A closed cell contains particles, which in this instance are merely suspended in air. The signal from the microphone is amplified by a lock-in amplifier referenced to the frequency and phase of the light chopper. By rotating the detector arm in the scattering plane angular scattering could also be measured. If a focused laser beam were used as the light source, absorption by single particles could conceivably be measured, and scattering combined with this absorption to give extinction. An advantage of the photoacoustic method is that the sensitivity of the detector, a microphone, in no way depends on the wavelength of the light.

Absorption by particles, for example acetylene smoke (Roessler and Faxvog, 1979a) and diesel emissions (Faxvog and Roessler, 1979), has been measured by the photoacoustic method.

11.7.5 Microwave Extinction Measurements

There undoubtedly have been many studies—many of which are probably classified—of absorption and scattering of microwaves by all kinds of objects,

particularly large objects such as aircraft and missiles. We have not thoroughly searched for all papers relevant to microwave scattering because our main interest has been in infrared to ultraviolet radiation. There is, however, a series of microwave experiments undertaken primarily to understand scattering of much shorter wavelength light by particles of comparable size, but by exploiting the inherent advantages of microwaves.

Extinction and scattering of light by a particle of given shape depend only on the *ratio* of a characteristic dimension (for a sphere, its radius) to the wavelength and the refractive index at that wavelength. Because of this similarity principle, scattering of visible light by small particles ($\sim 1\ \mu$m) may be studied by using microwaves and much larger particles (~ 10 cm) with the same shape and refractive index as the particles of interest. This *microwave analog technique* is discussed further in Section 13.3.

The essential ingredients of a microwave extinction experiment are shown in Fig. 11.22. The particle is suspended by threads so that its orientation can be changed and it can be moved in and out of the beam. Extinction is most conveniently determined in this instance by measuring the magnitude and phase of the forward-scattering amplitude and obtaining the cross section from the optical theorem (3.24). The experiment consists of nulling the detector (both amplitude and phase) with no scatterer present and then measuring the additional amplitude and phase of the forward-scattered wave with the particles inserted in the beam; calibration is accomplished with spheres of known size and refractive index.

The obvious advantage of the microwave experiment is that oriented single particles of arbitrary shape and, within limits, arbitrary refractive index, can be studied easily. Multilayered and other inhomogeneous particles pose no particular problems.

Microwave ($\lambda = 3$ cm) extinction measurements for beams incident parallel ($\zeta = 0°$) and perpendicular ($\zeta = 90°$) to the symmetry axis of prolate spheroids

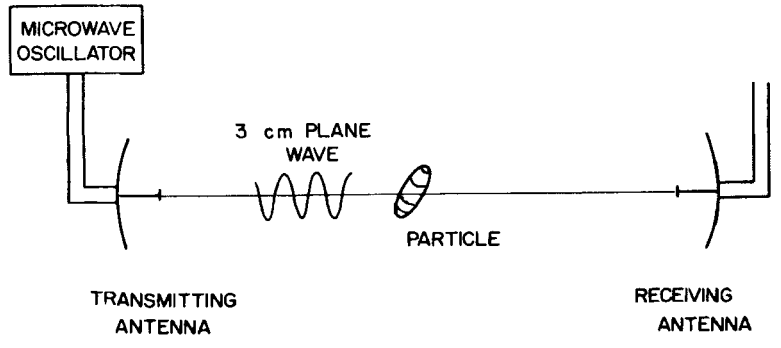

Figure 11.22 Schematic diagram of the microwave analog technique for measuring extinction by single oriented particles.

of varying semimajor axis a, but constant elongation $a/b = 2$, are shown in Fig. 11.23. These curves were taken from the paper by Greenberg et al. (1961), although a few notational changes were made for the sake of consistency. The general characteristics of this measured extinction are similar to those calculated for spheroids (Figs. 11.15 and 11.16). When the beam is incident perpendicular to the symmetry axis the extinction peaks are broad, and the ripple structure for TM polarization appears somewhat more pronounced than that for TE polarization. When the beam is incident parallel to the symmetry axis the extinction peak narrows and shifts to a smaller size parameter. The same kind of behavior is evident in the extinction curve for infinite cylinders (Fig. 11.17).

Extinction by a cylinder of the same material and with the same elongation as the spheroid, also measured by Greenberg et al., is shown in Fig. 11.24. Not surprisingly, extinction by the cylinder and spheroid are qualitatively similar. Infinite cylinder calculations agree rather well with measurements even for such a short cylinder. Additional experiments by Greenberg et al. suggest that such calculations tend to agree better with measurements if the length-to-diameter ratio is greater than about 5. Although the two extinction efficiencies (TE and TM) do not separately approach the infinite cylinder limits uniformly with increasing elongation (they oscillate about these values), the *difference* between the efficiencies more nearly does. Thus, there is some experimental evidence to support the assertions near the end of Section 8.4, made on the basis of

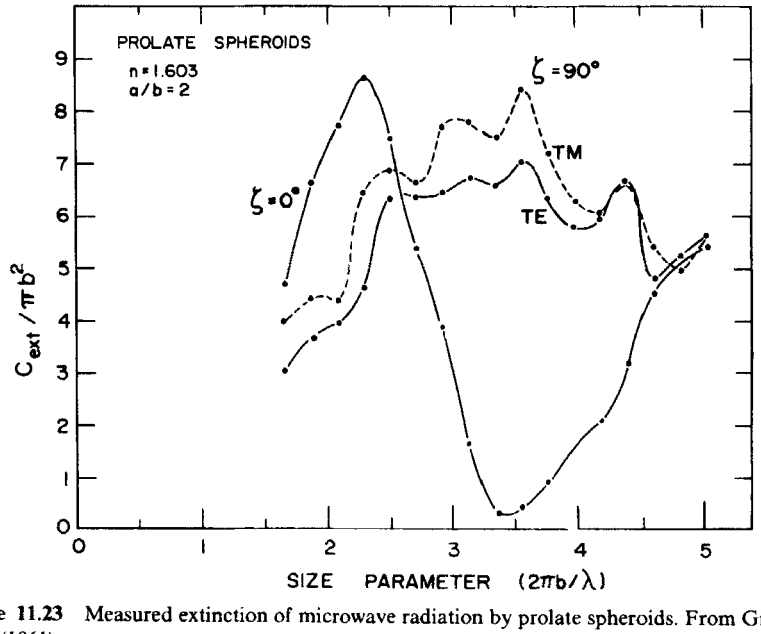

Figure 11.23 Measured extinction of microwave radiation by prolate spheroids. From Greenberg et al. (1961).

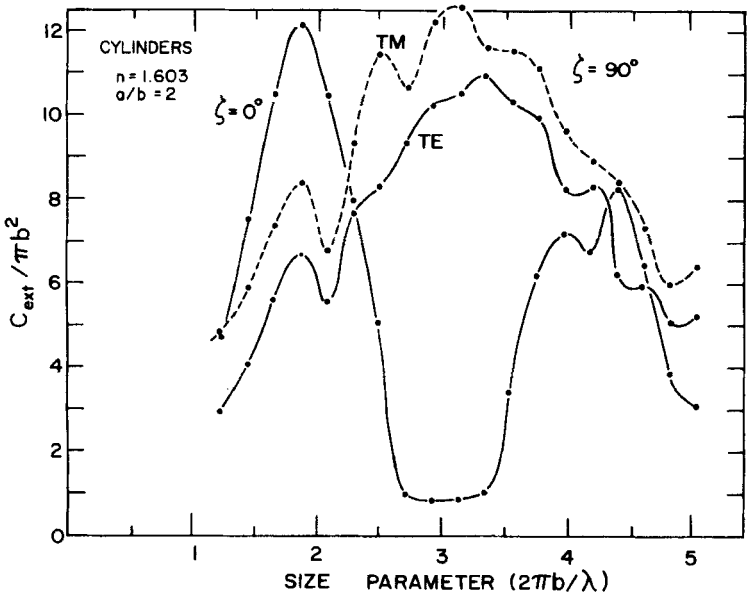

Figure 11.24 Measured extinction of microwave radiation by cylinders. From Greenberg et al. (1961).

diffraction theory, about when a finite cylinder may be considered effectively infinite. Of course, differences will always remain between finite and infinite cylinders with the same diameter and composition. The extent to which the former may be approximated by the latter will depend on the physical quantity of interest (extinction, angular scattering) and the desired accuracy.

11.8 EXTINCTION: A SYNOPSIS

Mie theory does an admirable job of predicting extinction by spherical particles with known optical constants: even the finest details it predicts—ripple structure—have been observed in extinction by single spheres. Several different causes—a distribution of sizes or shapes, and absorption—have the same effect of effacing the ripple structure or even the broader interference structure.

Absorption dominates over scattering for sufficiently small absorbing particles. Volumetric extinction by such particles is independent of their size but not of their shape; we shall discuss shape effects further in the following chapter.

Extinction is frequently dominated by scattering if the particle is about the same size as or larger than the wavelength. But absorption, which is usually manifested by absorption bands or absorption edges, can strongly affect extinction in unexpected ways: extinction may either increase or decrease with

increasing absorption, and symmetric absorption bands in bulk matter may be transformed into highly asymmetric or even inverted extinction bands in small particles.

Extinction is easy to measure in principle but may be difficult in practice, especially for large particles where it becomes difficult to discriminate between incident and forward-scattered light. Spheres and ensembles of randomly oriented particles do not linearly polarize unpolarized light upon transmission. But single elongated particles or oriented ensembles of such particles can polarize unpolarized light by differential extinction.

NOTES AND COMMENTS

Asymptotic expressions for extinction and absorption efficiencies of spheres averaged over a size parameter interval $\Delta x \sim \pi$ (i.e., with no ripple structure) have been derived by Nussenzveig and Wiscombe (1980).

Further discussion of extinction by oriented particles is given in van de Hulst (1957, Chaps. 15 and 16).